Research Article

Luan Thanh Pham*, Ahmed M. Eldosouky, David Gómez-Ortiz, Van-Hao Duong, Kamal Abdelrahman, and Hassan Alzahrani

Performance comparison of the wavenumber and spatial domain techniques for mapping basement reliefs from gravity data

https://doi.org/10.1515/geo-2020-0321
received August 18, 2021; accepted November 24, 2021

Abstract: Estimating the density interface depth is an important task when interpreting gravity data. A range of techniques can be applied for this. Here we compare the effectiveness of the wavenumber and spatial domain techniques for inverting gravity data with respect to basement reliefs. These techniques were tested with two synthetic gravity models, and then applied to a real case: the gravity data of the Magura basin (East Slovakian Outer Carpathian). The findings show that the spatial domain technique can precisely estimate the structures, but the computation speed is slow, while the wavenumber domain technique can perform faster computations with less precision.

Keywords: gravity inversion, wavenumber domain technique, spatial domain technique, Magura basin

1 Introduction

Analysis of gravity anomalies was the first geophysical method to be applied for hydrocarbon exploration. Despite being overshadowed by seismic methods, the gravity methods still have a significant role in some exploration areas, for example when mapping basement interfaces from gravity data. Several authors used the Euler deconvolution, as an automated method to detect the depth to gravity source [1–3]. Some other studies have used spectral analysis methods to estimate the density interfaces [4–6]. The major disadvantages of these techniques are that they depend on the structural index or the window size [7]. Another method, the wavenumber domain technique, can be used to overcome these problems. This technique is derived from the relationship between the Fourier transform of the gravity data and the Fourier transform of the sum of the depth powers. In recent years, the applications of the wavenumber domain technique to gravity anomalies have shown great success [8–11]. Aside from the wavenumber domain technique, the spatial domain technique, which utilizes the stacked prism model [12], is also widely and successfully used to map density structures, especially subsurface structures [13–17].

The concept of gravity inversion is not limited to the methods given above. Several authors have presented different methods to determine the geometry of a density interface related to the observed gravity anomaly [18–24]. In view of such an abundance of methods available, it is appropriate to revisit the applicability of popular gravity inversion methods for computation of basement depths of sedimentary basins.

The present study focuses on comparing the effectiveness of the wavenumber and spatial domain techniques for inverting gravity data. The techniques have been tested for both their practical application and accuracy on synthetic gravity data from two models and on real data from the Magura basin (East Slovakian Outer Carpathian).

2 Methods

2.1 The wavenumber domain technique [25]

The wavenumber technique is derived from the relationship between the Fourier transform of the gravity data

* **Corresponding author: Luan Thanh Pham,** Department of Geophysics, Faculty of Physics, University of Science, Vietnam National University, Hanoi, Vietnam, e-mail: luanpt@hus.edu.vn
Ahmed M. Eldosouky: Geology Department, Faculty of Science, Suez University, Suez, 43518, Egypt
David Gómez-Ortiz: Department of Biology and Geology, Physics and Inorganic Chemistry, ESCET, Universidad Rey Juan Carlos, Móstoles, Madrid, Spain
Van-Hao Duong: Geophysics Department, Hanoi University of Mining and Geology, Hanoi 100000, Vietnam
Kamal Abdelrahman, Hassan Alzahrani: Department of Geology & Geophysics, College of Science, King Saud University, P.O. Box 2455, Riyadh 11451, Saudi Arabia

and the Fourier transform of the sum of powers of the depth to the basement. Based on Parker's forward formula [26], Gao and Sun [27] derived the expression of the gravity effect of a density interface with the z-axis directed downward:

$$\Delta g = F^{-1}\left[2\pi\gamma(\rho_{\text{below}} - \rho_{\text{above}})\mathrm{e}^{(-|k|z_0)} \times \sum_{n=1}^{\infty}\frac{(|k|)^{n-1}}{n!}F[(-h)^n]\right]. \quad (1)$$

Here equation (1) can be rewritten as:

$$\Delta g = F^{-1}\left[2\pi\gamma\Delta\rho\mathrm{e}^{(-|k|z_0)}\sum_{n=1}^{\infty}\frac{(-|k|)^{n-1}}{n!}F[h^n]\right], \quad (2)$$

where $\Delta\rho = (\rho_{\text{above}} - \rho_{\text{below}})$ is the (negative) density contrast of the sediments relative to the basement, γ is the gravitational constant, h is the depth at the reference depth z_0, k is the frequency, and $F[\,]$ and $F^{-1}[\,]$ symbolize the Fourier and inverse Fourier transforms, respectively.

Based on equation (2), we can derive the gravity anomaly for the basin structure shown in Figure 1a by adding the Bouguer slab term $2\pi\gamma\Delta z_0$:

$$\Delta g = 2\pi\gamma\Delta\rho z_0 + F^{-1}\left[2\pi\gamma\Delta\rho\mathrm{e}^{(-|k|z_0)}\sum_{n=1}^{\infty}\frac{(-|k|)^{n-1}}{n!}F[h^n]\right]. \quad (3)$$

Here as illustrated in Figure 1, equation (3) can be better understood as breaking the basin model (Figure 1a) into two parts: an uneven layer with average depth z_0 (Figure 1b) and a layer confined between two horizontal levels with thickness z_0 (Figure 1c).

A simple rearrangement of equation (3) readily leads to:

$$h = F^{-1}\left[\frac{F[\Delta g - 2\pi\gamma\Delta\rho z_0]\mathrm{e}^{|k|z_0}}{2\pi\gamma\rho} - \sum_{n=2}^{\infty}\frac{(-|k|)^{n-1}}{n!}F[h^n]\right]. \quad (4)$$

Then, the basement depth can be estimated from equation (4) by an iterative inversion procedure. The procedure starts by setting $h = 0$. Using the inverse Fourier transform of the first term in equation (4) leads to the first estimates of the basement depth. This initial approximation is then used to calculate the new depth estimates. Updating for the new depth estimates continues until the RMS error between two successive depth estimates is smaller than an allowable value. The RMS error is given by:

$$\text{RMS} = \sqrt{\frac{\sum_{i=1}^{M}\sum_{j=1}^{N}(h_{i,j}^{t+1} - h_{i,j}^{t})^2}{M \times N}}, \quad (5)$$

where t is the iteration step, M and N are the point numbers in directions due north and east.

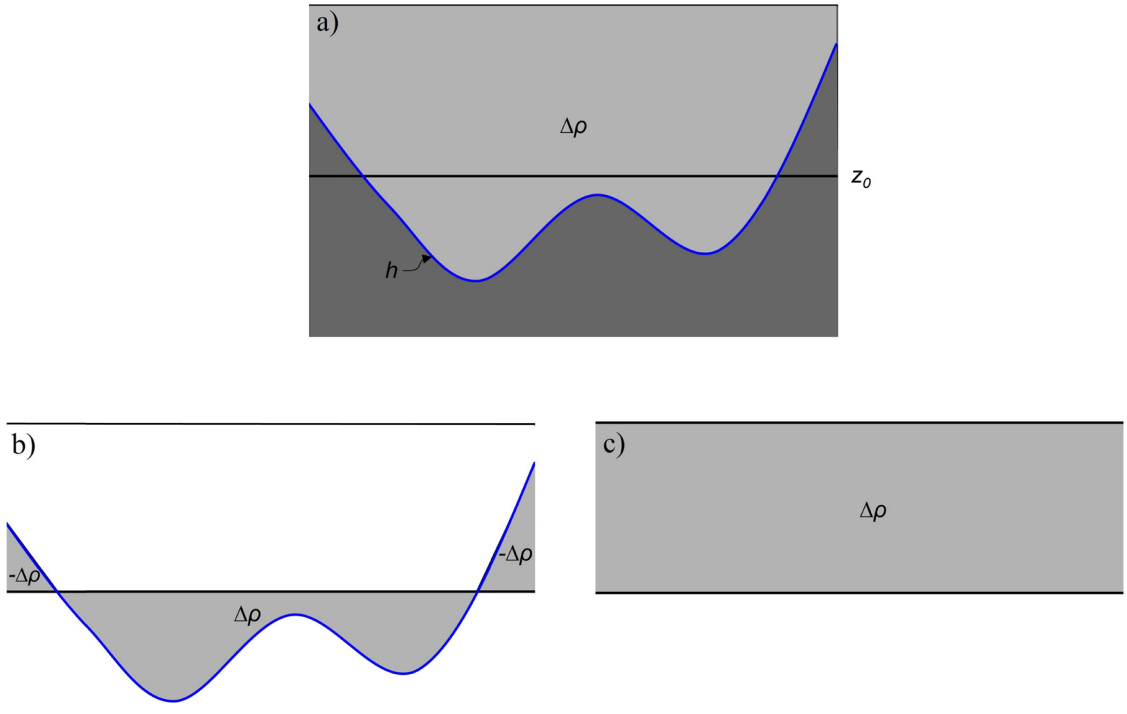

Figure 1: Equation (3) understood as breaking a basin model into two parts.

To ensure the convergence of the procedure, a low-pass filter $B(k)$ is applied during the calculation. The filter is given by [25]:

$$B(k) = \begin{cases} 1 & |k/2\pi| < \mathrm{WH} \\ \frac{1}{2}\left[1 + \cos\left(\frac{k - 2\pi WH}{2(SH - WH)}\right)\right] & \mathrm{WH} \le |k/2\pi| \le \mathrm{SH}, \\ 0 & |k/2\pi| > \mathrm{SH} \end{cases} \tag{6}$$

where WH and SH are frequencies of the filter. This filter passes frequencies lower than WH, cuts off the values larger than SH, and partly passes the values between WH and SH.

2.2 The spatial domain technique [12]

The spatial technique is based on dividing the sedimentary basin into rectangular prisms [12]. The initial depth approximations of the basin are computed assuming that the gravity data at each observed point is caused by an infinite horizontal slab, i.e.,

$$h^1 = \frac{\Delta g}{2\pi\gamma\Delta\rho}. \tag{7}$$

The theoretical gravity data at any observation is then computed from the initial approximations from equation (7), as:

$$\Delta g_{\mathrm{calc}} = \sum_{i=1}^{M}\sum_{j=1}^{N}\Delta g_{\mathrm{Prism}}(i,j), \tag{8}$$

where $\Delta g_{\mathrm{Prism}}$ is the gravity effect of a prism, which can be calculated using the formula as [28]:

$$\Delta g_{\mathrm{Prism}} = \gamma \int_{z=Z_1}^{Z_2}\int_{v=-W}^{W}\int_{u=-T}^{T}\frac{\Delta Z\,du\,dv\,dz}{r^3}, \tag{9}$$

where $r = \sqrt{(u-x)^2 + (v-y)^2 + z^2}$, Z_1 and Z_2 are the top and bottom depths, and T and W are the half thickness and half width of the prism, respectively.

Thus, the gravity effect of a prism can be written as [28,29]:

$$\Delta g_{\mathrm{Prism}} = G\Delta\rho\left(z\ a\tan\frac{XY}{zR} + \frac{X}{2}\ln\frac{R-Y}{R+Y} + \frac{Y}{2}\ln\frac{R-X}{R+X}\right)\Bigg|_{X_1}^{X_2}\Bigg|_{Y_1}^{Y_2}\Bigg|_{Z_1}^{Z_2}, \tag{10}$$

where

$$X_1 = x + T,\ X_2 = x - T,\ Y_1 = y + W,\ Y_2 = y - W,$$
$$R = \sqrt{X^2 + Y^2 + z^2}.$$

Using the differences between the observed and computed anomalies, the depth estimates can be improved by the Gauss–Newton method as [12,15]:

$$h^{(t+1)} = \frac{\Delta g - \Delta g^{(t)}_{\mathrm{calc}}}{2\pi\gamma\Delta\rho} + h^{(t)}, \tag{11}$$

where t is the iteration number

Updating for the new depth estimates continues until the RMS error between the observed and computed anomalies is smaller than an allowable value.

3 Models

The effectiveness of the wavenumber and spatial domain techniques was tested with two models. The first was a smooth basin model having a density contrast of $-0.2\ \mathrm{g/cm^3}$. Figure 2a and b shows the 3D and plan views of the interface topography of the model. Figure 2c shows the theoretical gravity data of the model calculated on a 64×64 mesh grid with 1 km intervals. Note that the gravity computed by the wavenumber and spatial domain techniques are the same. For the wavenumber domain technique, the choice of a proper SH/WH can be obtained by power spectrum analysis of gravity anomaly data. A plot of the logarithm of the power spectrum versus wavenumber usually shows several linear segments that decrease in slope with increase in wavenumber. Generally, low radial wavenumbers mostly correspond to deep sources, and intermediate radial wavenumbers mainly relate to shallower ones, while high radial wavenumbers are dominated by noise [30,31]. On the other hand, Pustisek [32] showed that a low pass filter with a theoretical cutoff frequency SH $\le 1/L$ (where L is maximum of the topographic relief function h) can be used to ensure the convergence of the iterative procedure [32]. In fact, the mean depth of the density interface can also be estimated directly from the slope of the logarithm of the power spectrum or other geophysical/geological information. Caratori Tontini et al. [33] showed that a good compromise can be chosen as WH = 0.5SH [33]. In the synthetic model, we used a known average depth of 1.6 km, and the frequency parameters were determined in a way similar to those determined by Pustisek [32] and Caratori Tontini et al. [33] (i.e., SH = $0.3\ \mathrm{km^{-1}}$ and WH = $0.15\ \mathrm{km^{-1}}$) [32,33]. Figure 3a and b displays the depths obtained from the wavenumber and spatial domain techniques, respectively. Here the wavenumber domain algorithm converged after five iterations. It stopped when the RMS error between two

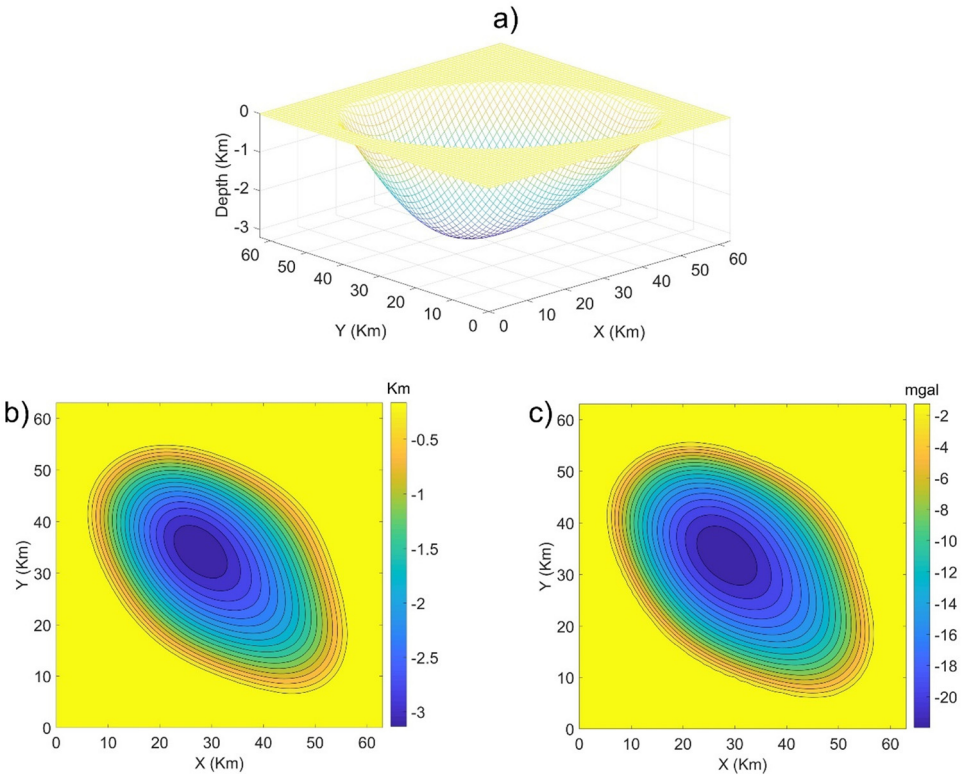

Figure 2: (a) Perspective view of the first basin, (b) 2D view of the basin, and (c) gravity anomaly of the basin.

successive approximations dropped below a pre-assigned error of 10^{-3} km. Using a threshold value of the convergence criteria of 0.04 mGal, the inversion scheme of the spatial domain technique required 4 iterations for the convergence of the computed anomalies to the observed anomalies. Figure 3c displays the differences between the model depths and the inverted depths as calculated by the wavenumber technique. These differences ranged from −0.1559 to 0.1596 km, with an RMS error of 0.0572 km. Figure 3d displays the differences between the model depths and the inverted depths as calculated by the spatial domain techniques, which ranged from – 0.0358 to 0.0150 km, with an RMS error of 0.0064 km. Clearly, both techniques are effective in estimating the depth to the basement. Comparing Figure 3c and d, however, it can be seen that the spatial domain technique delivers a more precise result. On the other hand, the wavenumber technique took only 0.1543 s to invert the gravity data in a personal computer with Core(TM) i7 at 2.7 GHz CPU, while the spatial domain technique took 48.0705 s. Figure 3e and f shows the gravity anomalies calculated from inferred structures in Figure 3a and b by the forward formulas of the wavenumber domain technique (equation [3]) and spatial domain technique (equation [10]), respectively. Figure 3g displays the differences between the anomalies calculated by the wavenumber domain technique and the theoretical anomalies, with the differences ranging from –1.1453 to 0.8862 mGal, with an RMS error of 0.3945 mGal. Figure 3h displays the differences between the anomalies calculated by the spatial domain technique and the theoretical anomalies, which ranged from –0.0652 to 0.1455 mGal, with an RMS error of 0.0295 mGal. Clearly, the anomalies obtained from inferred structures by the spatial domain technique (Figure 3f) are closer in shape to the theoretical anomalies than the anomalies in Figure 3e.

The second model is a basin with more abrupt topography. The 3D and ground views of the interface topography of the model are displayed in Figure 4a and b, respectively. Figure 4c shows the theoretical gravity anomalies of the model, with a density contrast of $-0.2\ \mathrm{g/cm^3}$ calculated on a 64 × 64 mesh grid with 1 km intervals. In this case, to invert the anomalies by means of the wavenumber domain technique, we used an average depth of 3.3 km, and the frequency parameters of the filter were selected as SH = $0.12\ \mathrm{km^{-1}}$ and WH = $0.06\ \mathrm{km^{-1}}$ [32,33]. Figure 5a and b displays the results determined by the wavenumber and spatial domain techniques, respectively. Figure 5c displays the differences between the model depths and the inverted depths as calculated by the wavenumber technique, which range from –1.0020 to 0.5047 km with an

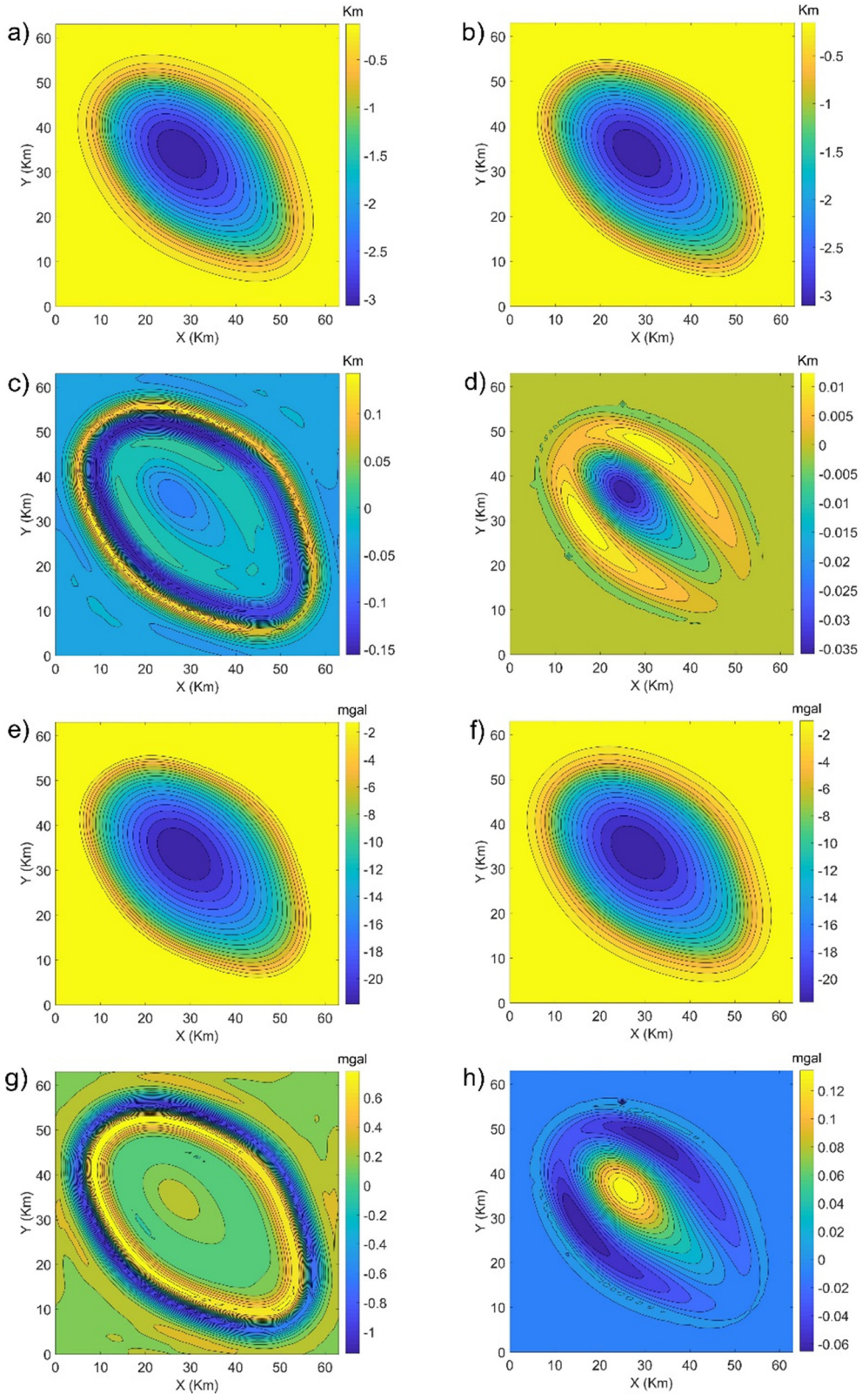

Figure 3: (a) The computed depths by wavenumber domain technique, (b) the estimated depths by spatial domain technique, (c) the difference between the computed depths in (a) and model depths, (d) the difference between the computed depths in (b) and model depths, (e) the gravity data calculated from inferred structures in (a), (f) the gravity data calculated from inferred structures in (b), (g) the difference between the computed anomalies in (a) and theoretical gravity data, (h) the difference between the computed anomalies in (b) and theoretical anomalies.

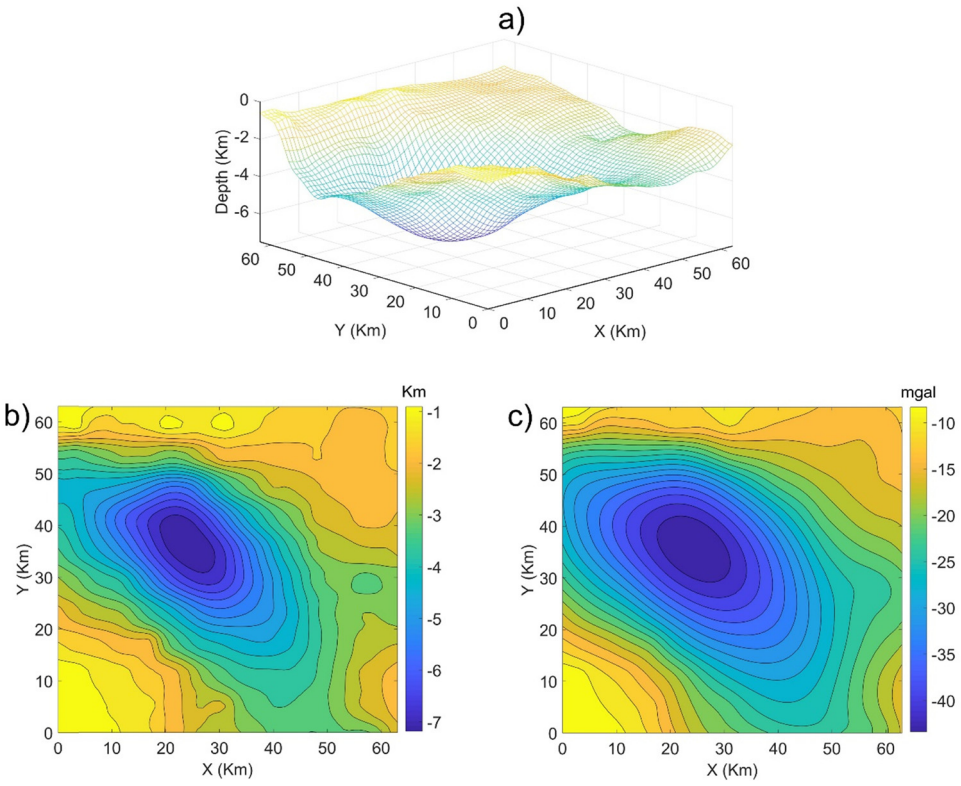

Figure 4: (a) Perspective view of the second basin, (b) 2D view of the basin, and (c) gravity anomaly of the basin.

RMS error of 0.2501 km. Figure 5d displays the differences between the model depths and the inverted depths as calculated by the spatial domain technique, which range from −0.2117 to 0.2453 km with an RMS error of 0.0522 km. Although both methods are effective in determining the depth to the basement, the spatial domain method generates more accurate result. In this case, the wavenumber domain method is about 593 times faster than the spatial domain method. Figure 5e and f shows the anomalies calculated from detected structures in Figure 5a and b by the forward formulas of the wavenumber and spatial domain technique, respectively. Figure 5g displays the differences between the anomalies calculated by the wavenumber domain technique and the theoretical anomalies, which ranged from −0.9611 to 4.5691 mGal, with an RMS error of 1.5250 mGal. Clearly, there is a significant difference between these gravity data. Figure 5h displays the differences between the anomalies calculated by the spatial domain technique and the theoretical anomalies, which were in the range of −0.2308 to 0.3598 km with an RMS error of 0.0764 km. Note that the gravity data calculated through the spatial domain technique is not significantly different from the theoretical results.

To estimate the effects of the density contrast $\Delta\rho$, level z_0 and low pass filter (WH, SH) on the gravity inversion using the wavenumber domain technique, the gravity anomaly of the second model has been inverted for different assumed values of $\Delta\rho$, z_0 and parameters WH and SH of the low pass filter. The RMS errors between the model and inverted depths are shown in Table 1. We can see that, the wavenumber domain technique is less sensitive to the values of the average depth, but more sensitive to the values of the density contrast. Although all inversions converged with the different filters, the difference between the model and inverted depths is significant when using the small values of WH and SH. The reason is that the use of the low pass filter leads to a significant loss of high frequency information, so the inverted basement interface does not match with that of the model depth. Since the spatial domain technique does not require average depth and low pass filter, we only estimate the effects of the density contrast $\Delta\rho$ on the gravity inversion. The RMS errors between the model depth and the depths determined from using different assumed values of $\Delta\rho$ are also shown in Table 1. It is numerically verified that as the density contrast increases or decreases, the difference between the model and inverted depths increases rapidly. These results suggest that the spatial domain technique is more sensitive to the values of the density contrast than the wavenumber domain technique. Recently, Florio [21]

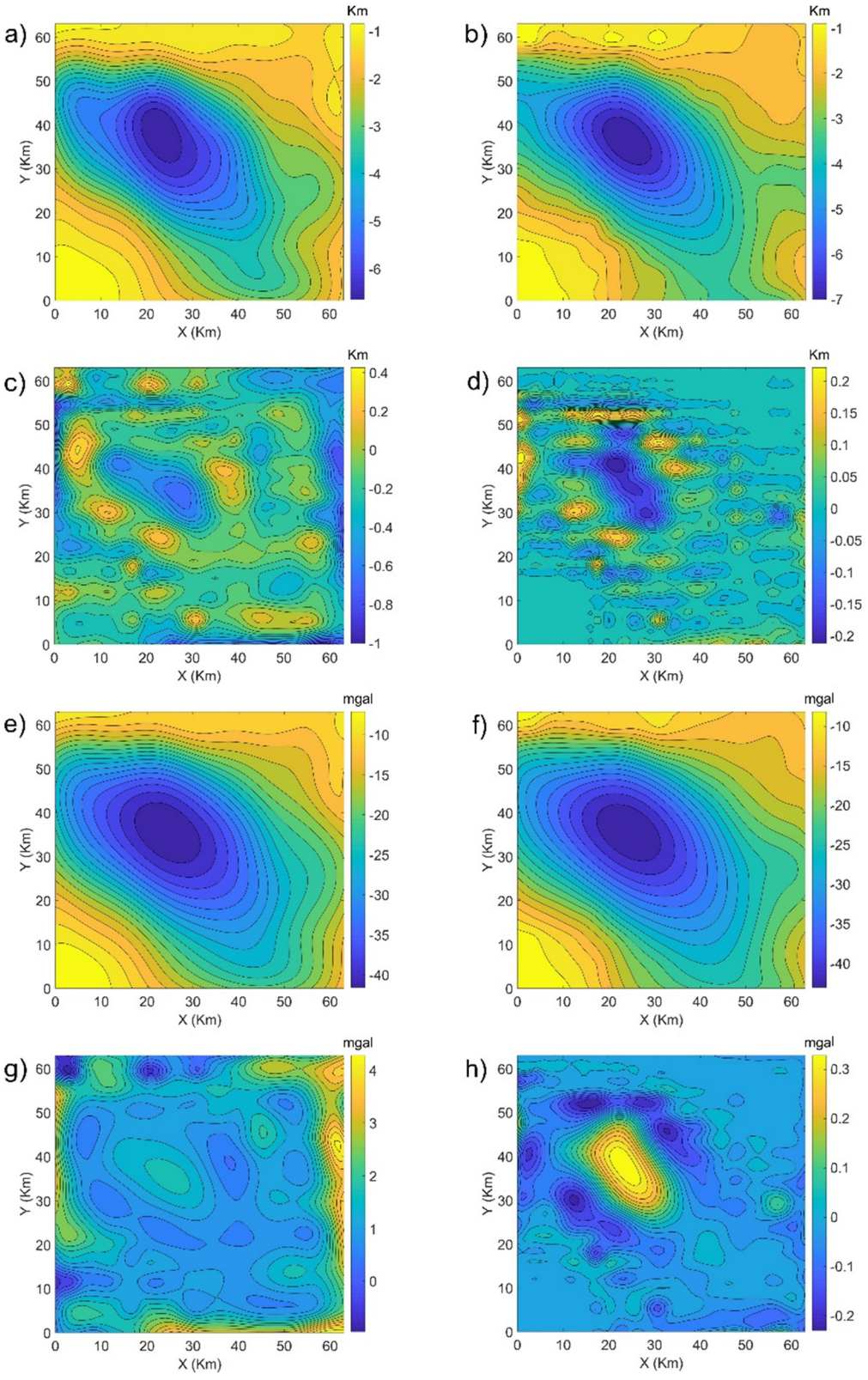

Figure 5: (a) The computed depths by wavenumber domain technique, (b) the estimated depths by spatial domain technique, (c) the difference between the computed depths in (a) and model depths, (d) the difference between the computed depths in (b) and model depths, (e) the gravity data calculated from inferred structures in (a), (f) the gravity data calculated from inferred structures in (b), (g) the difference between the computed anomalies in (a) and theoretical gravity data, (h) the difference between the computed anomalies in (b) and theoretical anomalies.

Table 1: RMS errors between the model and the inverted depths

Z_0 (km)	2.7	3	3.3	3.6	3.9
RMS from the wavenumber domain method (km)	0.2605	0.2536	0.2501	0.2507	0.2566
RMS obtained from the spatial domain (km)	—	—	—	—	—
Density (g/cm^3)	**0.16**	**0.18**	**0.20**	**0.22**	**0.24**
RMS from the wavenumber domain method (km)	0.7545	0.3310	0.2501	0.4741	0.7011
RMS obtained from the spatial domain (km)	0.9740	0.4237	0.0522	0.3239	0.5823
WH and SH (km^{-1})	**0.02; 0.04**	**0.04; 0.08**	**0.06; 0.12**	**0.08; 0.16**	**0.10; 0.20**
RMS from the wavenumber domain method (km)	0.4943	0.2911	0.2501	0.2514	0.2739
RMS obtained from the spatial domain (km)	—	—	—	—	—

has developed a method for inverting gravity data, which does not require a value of density contrast [21]. The application of this method to the gravity data has shown great success in determining the basement relief of the Yucca Flat basin, but it requires several depth constraints at some locations in the study area, which can be basement depth data from well data or interpreted seismic sections.

To further test the effectiveness of the wavenumber and spatial domain methods in the presence of errors, we added Gaussian noise with different noise levels to synthetic gravity anomaly of the second model. Figure 6a shows the synthetic data corrupted by Gaussian noise with standard deviation of 0.1 mGal. Figure 6c and e shows the computed depths by the wavenumber domain technique and spatial domain techniques, respectively. Figure 6b shows the synthetic data corrupted by Gaussian noise with standard deviation of 0.2 mGal. Figure 6d and f shows the computed depths by the wavenumber domain technique and spatial domain techniques, respectively. We can see that the wavenumber domain technique is less sensitive to noise than the spatial domain technique. The wavenumber domain technique produces similar results for different noise levels, and these results closely match up with the result for the noise-free synthetic data (Figure 5a). The reason is that wavenumber domain technique require the use of a low pass filter to obtain convergence of the iterative process, such a filter can remove part of the high frequency content associated with noise in the data.

4 Magura basin (East Slovakian Outer Carpathian)

The applicability of the wavenumber and spatial domain techniques was also tested by interpreting real data from the Magura basin (East Slovakian Outer Carpathian). According to Svancara [13], the Magura sedimentary basin formed by slightly deformed porous Lower Oligocene Malcov beds lie on strongly deformed flysch rocks in Eocene and Paleocene of the Magura Nappe. Figure 7a shows the residual gravity data of the Magura basin, digitized from Svancara [13] on a 26 × 28 grid along the east and north directions. Figure 7a also shows the cross section SS′ of the basin where the gravity data were interpreted by Svancara [13] using a density contrast of −0.2 g/cm^3. Svancara [13] reported a maximum thickness of 0.48 km. To invert the anomalies using the wavenumber domain technique, we used an average depth of 0.2 km and selected the frequencies as SH = 1.8 km^{-1} and WH = 0.9 km^{-1}. In this case, the iterative process of the wavenumber domain algorithm performed 24 iterations to fall below a pre-assigned error of 10^{-3} km between 2 successive interface approximations. Using threshold value of the convergence criteria 0.015 mGal, the inversion scheme of the spatial domain technique required 4 iterations for the convergence of the computed anomalies to the observed anomalies. Figure 7b shows the basement depths determined by the wavenumber domain technique, with a maximum depth of 0.4264 km. Figure 7c displays the basement depths determined by the spatial domain technique, with a maximum depth of 0.4754 km. According to our depth configurations (Figure 7b and c), the basement depth gets deepest approximation related to a nearly E–W trending in the central region and gets shallower at surrounding regions. Although the basement structures determined from the two methods were quite similar, the wavenumber domain technique results in a smoother relief that may not represent the real relief (as shown in the second model). Here the wavenumber domain technique is about 16 times faster than the spatial domain technique. Figure 7d and e shows the gravity data calculated from the

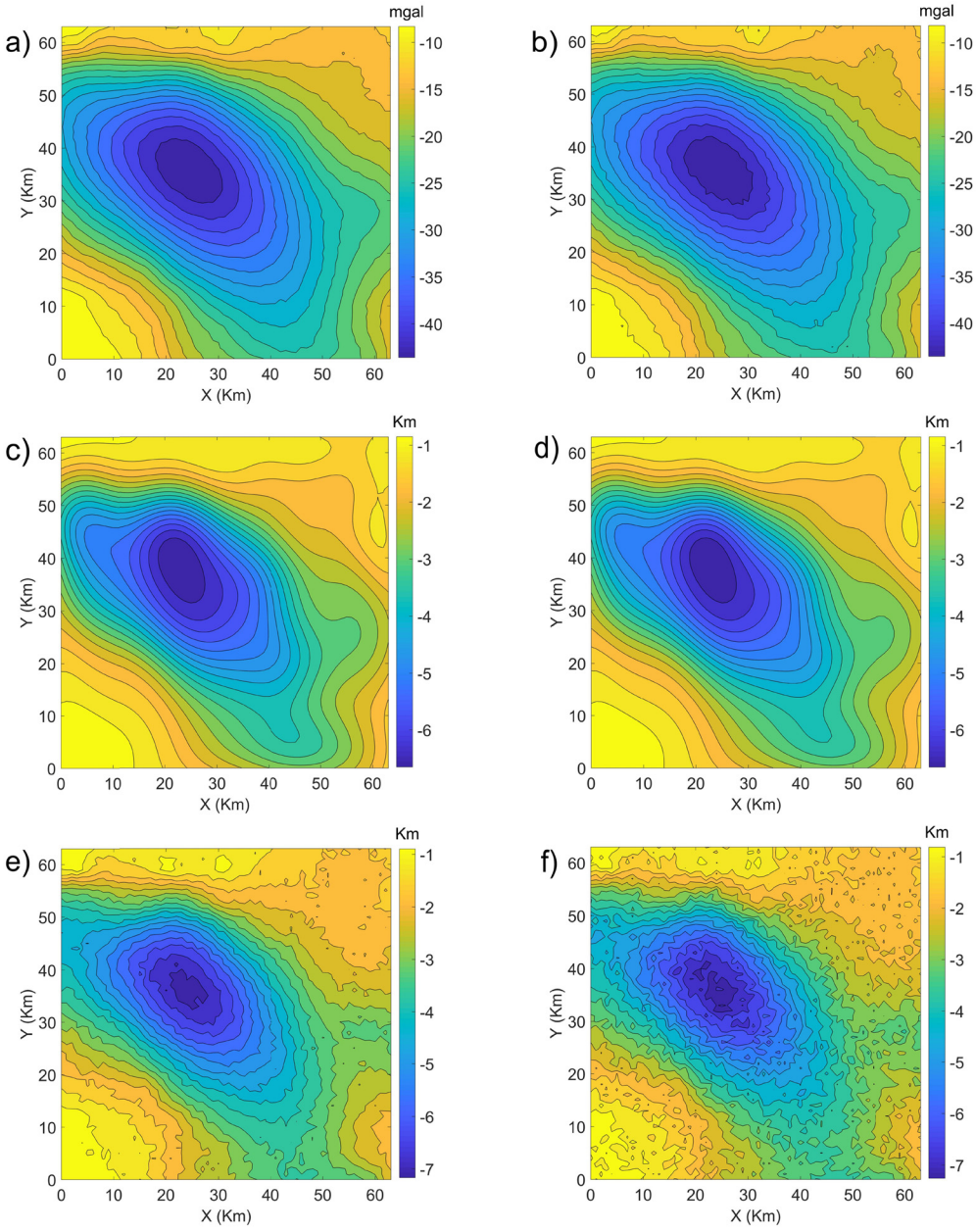

Figure 6: (a) The synthetic data corrupted by Gaussian noise with standard deviation of 0.1 mGal, (b) the synthetic data corrupted by Gaussian noise with standard deviation of 0.2 mGal, (c) the result obtained from applying the frequency domain technique to gravity data in (a), (d) the result obtained from applying the frequency domain technique to gravity data in (b), (e) the result obtained from applying the spatial domain technique to gravity data in (a), and (f) the result obtained from applying the spatial domain technique to gravity data in (b).

detected structures in Figure 7d and c by the forward formulas of the wavenumber and spatial domain techniques, respectively. Figure 7f shows the differences between the anomalies calculated by the wavenumber domain technique and the residual data, which ranged from −0.1050 to 0.1789 mGal with the RMS error being 0.0505 mGal. Figure 7h shows the differences between the anomalies calculated by the spatial domain technique and the residual data. These differences were less than 0.1423 mGal, with an RMS error of only 0.0150 mGal. The fit between the calculated and residual gravity data indicates the validity of the model estimated by the spatial domain technique. On the other hand, the wavenumber domain technique required much less time.

For comparison, Figure 8b displays the structures inverted by the wavenumber and spatial domain techniques and the basin model inferred by Svancara [13] along the SS′ cross section. It can be observed from Figure 8a

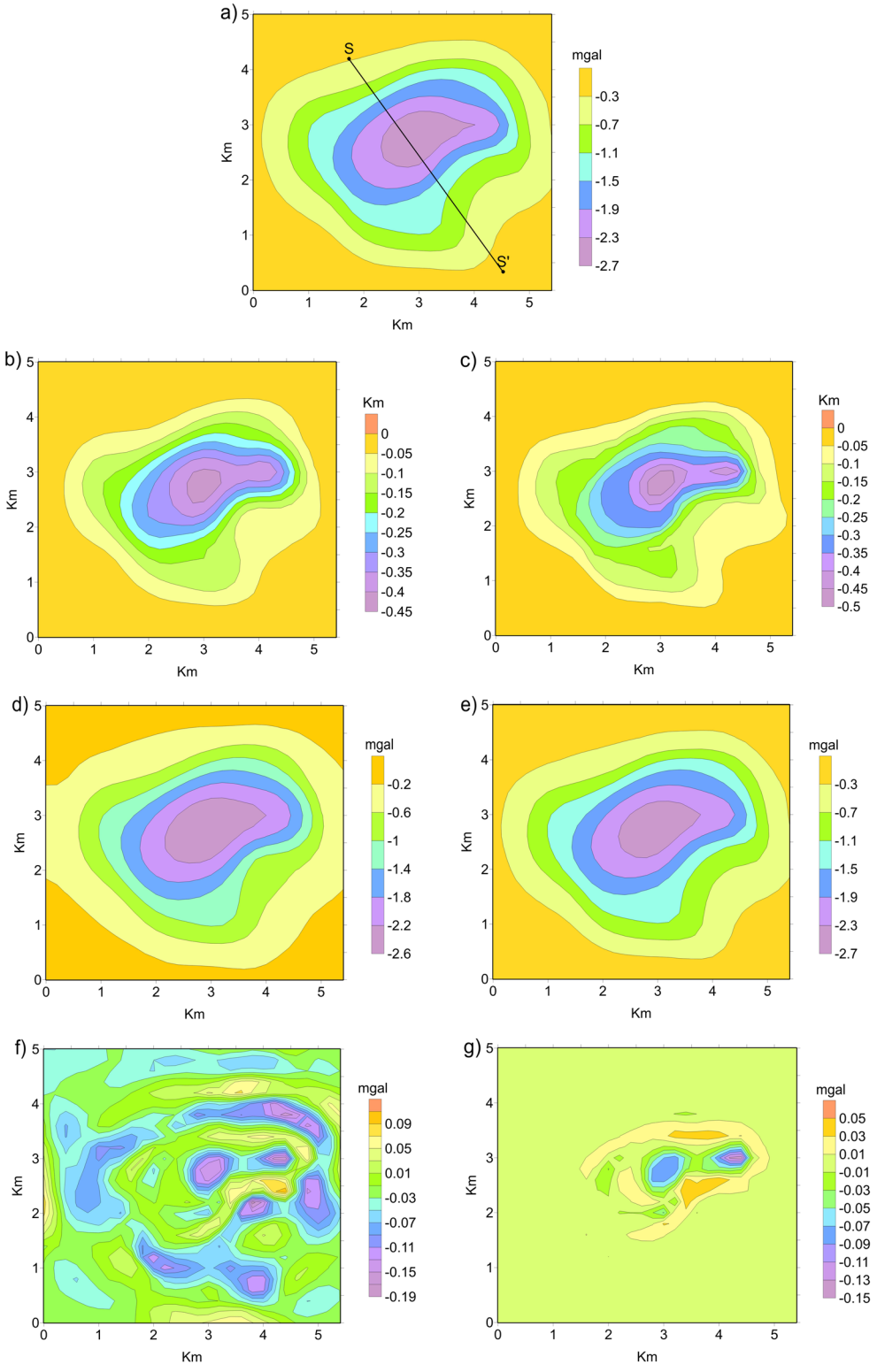

Figure 7: (a) The gravity anomalies of the Magura basin, (b) the estimated depths by wavenumber domain technique, (c) the estimated depths by spatial domain technique, (d) the gravity anomalies calculated from inferred structures in (b), (e) the gravity anomalies calculated from inferred structures in (c), (f) the difference between the computed anomalies in (d) and residual anomalies, (g) the difference between the computed anomalies in (e) and residual anomalies.

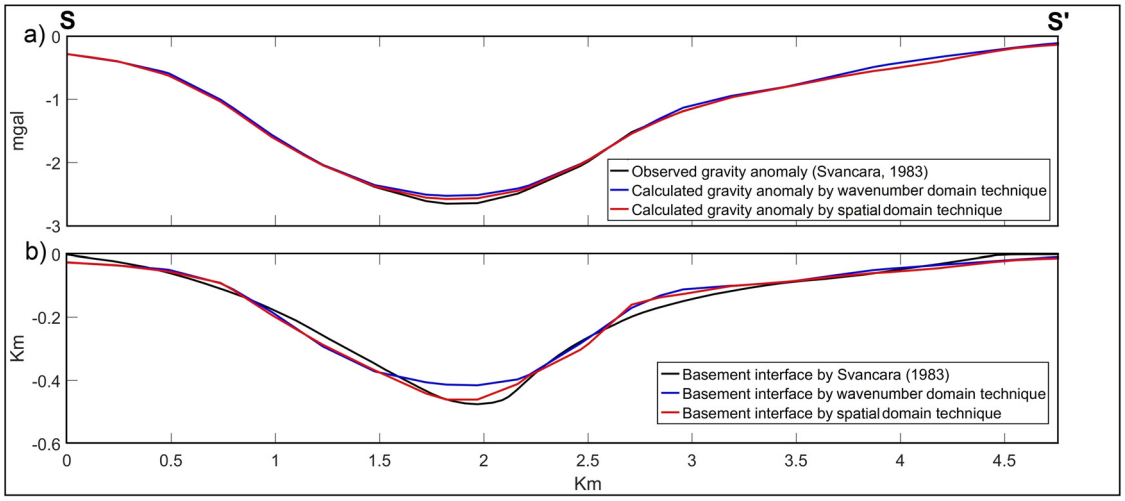

Figure 8: Interpretation of the gravity data on the cross section SS′.

that the modeled gravity data closely coincide with the real gravity data. The maximum depth of the basin on the profile determined by the wavenumber domain technique was 0.4160 km, whereas the spatial domain technique showed a maximum depth of 0.4612 km, which compares well with the figure of 0.4759 km reported by Svancara [13]. Although, by and large, the estimated structures coincide well with those reported by Svancara [13], those determined by the spatial domain technique (Figure 7c) were closer to the shape of Svancara's basin model than those determined by the wavenumber domain technique.

5 Conclusion

We have presented a comparative study of the effectiveness of the wavenumber and spatial domain techniques for inverting gravity data of basement reliefs. The effectiveness of these techniques is tested on both synthetic and real gravity anomalies. The obtained results showed that the spatial domain technique is more sensitive to density contrast and noise than the wavenumber domain technique. These results also showed that the wavenumber domain technique is less sensitive to the values of the average depth, but it is sensitive to the low pass filter when the SH and WH parameters are small. Both techniques successfully recovered the basement structures of the synthetic model when using the reasonable inputs. Similarly, when tested against a real case belonging to the Magura basin, the obtained structures coincide well with available structures. By comparing the results estimated by both techniques, it was found that the wavenumber domain technique required much less time but was less accurate, while the spatial domain technique has a slower computation speed, but is able to determine the basement depth precisely.

Acknowledgements: Deep thanks and gratitude to the Researchers Supporting Project number (RSP-2021/351), King Saud University, Riyadh, Saudi Arabia for funding this research article. This research has been done under the research project QG21.24 of Vietnam National University, Hanoi.

Conflict of interest: Authors state no conflict of interest.

References

[1] Beiki M. Analytic signals of gravity gradient tensor and their application to estimate source location. Geophysics. 2010;75(6):159–74.
[2] Tedla GE, van der Meijde M, Nyblade AA, van der Meer FD. A crustal thickness map of Africa derived from a global gravity field model using Euler deconvolution. Geophys J Int. 2011;187(1):1–9.
[3] Ghosh GK, Singh CL. Spectral analysis and Euler deconvolution technique of gravity data to decipher the basement depth in the Dehradun-Badrinath area. J Geol Soc India. 2014;83(5):501–12.
[4] Russo RM, Speed RC. Spectral analysis of gravity anomalies and the architecture of tectonic wedging. NE Venezuela Trinidad Tecton. 1994;13(3):613–22.
[5] Tiwari VM, Kumar RM, Mishra DC. Long wavelength gravity anomalies over India: Crustal and lithospheric structures and its flexure. J Asian Earth Sci. 2013;70–71:169–78.

[6] Ngalamo JFG, Sob M, Bisso D, Abdelsalam MG, Atekwana E, Ekodeck GE. Lithospheric structure beneath the Central Africa Orogenic Belt in Cameroon from the analysis of satellite gravity and passive seismic data. Tectonophysics. 2018;745(16):326–37.
[7] Aydın I, Oksum E. MATLAB code for estimating magnetic basement depth using prisms. Comput Geosci. 2012;46:183–8.
[8] Pham LT, Do TD, Oksum E, Le ST. Estimation of Curie point depths in the Southern Vietnam continental shelf using magnetic data. Vietnam J Earth Sci. 2019;41(3):216–28.
[9] Tugume F, Nyblade A, Julià J, van der Meijde M. Precambrian crustal structure in Africa and Arabia: Evidence lacking for secular variation. Tectonophysics. 2013;609:250–66.
[10] Oruç B, Gomez-Ortiz D, Petit C. Lithospheric flexural strength and effective elastic thicknesses of the Eastern Anatolia (Turkey) and surrounding region. J Asian Earth Sci. 2017;150:1–13.
[11] Xuan S, Jin S, Chen Y. Determination of the isostatic and gravity Moho in the East China Sea and its implications. J Asian Earth Sci. 2020;187:104098.
[12] Bott MHP. The use of rapid digital computing methods for direct gravity interpretation of sedimentary basins. Geophys J Roy Astron Soc. 1960;3:63–7.
[13] Svancara J. Approximate method for direct interpretation of gravity anomalies caused by surface three-dimensional geologic structures. Geophysics. 1983;48(3):361–6.
[14] Barbosa VCF, Silva JBC, Medeiros WE. Gravity inversion of a discontinuous relief stabilized by weighted smoothness constraints on depth. Geophysics. 1999;64(5):1429–37.
[15] Silva JBC, Santos DF, Gomes KP. Fast gravity inversion of basement relief. Geophysics. 2014;79(5):G79–91.
[16] Pallero JLG, Fernandez-Martinez JL, Bonvalot S, Fudym O. Gravity inversion and uncertainty assessment of basement relief via particle swarm optimization. J Appl Geophys. 2015;116:180–91.
[17] Chakravarthi V, Pramod Kumar M, Ramamma B, Rajeswara Sastry S. Automatic gravity modeling of sedimentary basins by means of polygonal source geometry and exponential density contrast variation: two space domain based algorithms. J Appl Geophys. 2016;124:54–61.
[18] Santos DF, Silva JBC, Martins CM, dos Santos RDCS, Ramos LC, de Araújo ACM. Efficient gravity inversion of discontinuous basement relief. Geophysics. 2015;80(4):G95–G106.
[19] Rossi L, Reguzzoni M, Sampietro D, Sansò F. Integrating geological prior information into the inverse gravity problem: the Bayesian approach. In Sneeuw N, Novàk P, Crespi M, Sansò F, (eds). VIII Hotine-Marussi Symposium on Mathematical Geodesy. vol. 142. Heidelberg, Germany: Springer, International Association of Geodesy Symposia; 2015. p. 317–24.
[20] Florio G. Mapping the depth to basement by iterative rescaling ofgravity or magnetic data. J Geophys Research: Solid Earth. 2018;123:9101–20.
[21] Florio G. The estimation of depth to basement under sedimentary basins from gravity data: review of approaches and the ITRESC method, with an application to the Yucca Flat basin (Nevada). Surv Geophys. 2020;41(5):935–61.
[22] Barzaghi R, Biagi L. The collocation approach to Moho estimate. Ann Geophys. 2014;57(1):S0190.
[23] Reguzzoni M, Sampietro D, Rossi L. The gravity contribution to the Moho estimation in the presence of vertical density variations. Rend Fis Acc Lincei. 2020;31:69–81.
[24] Reguzzoni M, Rossi L, Baldoncini M, Callegari I, Poli P, Sampietro D, et al. GIGJ: a crustal gravity model of the Guangdong Province for predicting the geoneutrino signal at the JUNO experiment. J Geophys Res . 2019;124(4):4231–49.
[25] Oldenburg DW. The inversion and interpretation of gravity anomalies. Geophysics. 1974;39(4):526–36.
[26] Parker RL. The rapid calculation of potential anomalies. Geophys J R Astronomical Soc. 1972;31:447–55.
[27] Gao X, Sun S. Comment on "3DINVER.M: A MATLAB program to invert the gravity anomaly over a 3D horizontal density interface by Parker-Oldenburg's algorithm." Comput Geosci. 2019;127:133–7.
[28] Nagy D. The gravitational attraction of a right rectangular prism. Geophysics. 1966;31(2):362–71.
[29] Rao DB, Prakash MJ, Ramesh, Babu N. 3-D and 21/2-D modeling of gravity anomalies with variable density contrast. Geophys Prospect. 1990;38:411–22.
[30] Spector A, Grant FS. Statistical models for interpreting aeromagnetic data. Geophysics. 1970;35:293–302.
[31] Pham LT, Oksum E, Gómez-Ortiz D, Do TD. MagB_inv: a high performance Matlab program for estimating the magnetic basement relief by inverting magnetic anomalies. Comput Geosci. 2020;134:104347.
[32] Pustisek AM. Noniterative three-dimensional inversion of magnetic data. Geophysics. 1990;55(6):782–5.
[33] Caratori Tontini F, Cocchi L, Carmisciano C. Potential-field inversion for a layer with uneven thickness: The Tyrrhenian Sea density model. Phys Earth Planet Inter. 2008;166(1–2):105–11.